Research Article

Qiang Li, Yu Jiang*, Yan Zhang, Yu Gao, Xiaohong Guo, Ruifei Cui, Sichen Wang, Wenming Guo, Tiexin Lv, Lifeng Cai, Lei Zhang, Xiaoying Li, and Haichen Lin

# Optimal attitude control for solar array orientation

https://doi.org/10.1515/astro-2021-0009
Received Sep 22, 2021; accepted Nov 08, 2021

**Abstract:** For low Earth orbit (LEO) satellites, solar panel is a firstly key device to convert the solar radiation into the electric power to supply the energy consume. However, the solar array is always suffering from the power degradation due to the harsh space environments. To meet the power balance in the end life of the spacecraft, attitude determination and control system (ADCS) plays an important role in the solar panel direction to change the solar energy input. Here, the solar cell performance parameters from an LEO satellite running on a dawn-dusk Sun synchronous orbit (SSO) are investigated. A yaw maneuver application is presented to satisfy the electric power supply (EPS) risk of the solar cell current decrease. Validated in the space operation, the results have shown that in the yaw mode, the EPS output is improved and the solar cell current is averagely enhanced more than 10% when the orbit incidence is 35°. The yaw maneuver is applied to the state of health (SOH) management with a better power supply. The solution can be widely and usefully taken into account to increase the solar array output for a near-Earth satellite in the risk of the power shortage.

**Keywords:** LEO satellite; solar panel; space environment

## 1 Introduction

In the near-Earth space exploration, solar power is required as a reliable energy source for satellites (Gueymard 2018; Espinet-Gonzalez *et al.* 2020). In space operation, after the launch and early orbit phase (LEOP) of a satellite, power supply management is one of the extremely important concerns for engineers. Solar panel is devised to supply the electric power with solar cell. Unfortunately, solar cell on orbit is always influenced by the harsh space environmental effects (SEEs) (Xapsos 2019; Kerr and MacDonald 2021; Lu and Shao 2019) with the power degradation.

Due to the displacement damage and cumulative radiation effects, a solar cell output decreases permanently and can be worse in a special or extreme space weather (Maurer *et al.* 2018; Hands *et al.* 2018) on several orbits including low Earth orbit (LEO), middle Earth orbit (MEO) and geosynchronous Earth orbit (GEO).

In the space plasma environments, the solar array surface may endure large potential differences and one of the considerations is the arc damage because of the electrostatic discharge (ESD) effects that may be destructive (Ferguson *et al.* 2020a,b; Keys *et al.* 2020). Frequent arcs can result in accelerating the solar cell degradation due to the glass cover adhesive ionization that may cause the molecular contamination (Ferguson *et al.* 2020a,b; Engelhart *et al.* 2019; Ferguson *et al.* 2019). These processes may be further exacerbated by the ultraviolet radiation effects (Toyoda *et al.* 2020). Thickening the glass cover can slow down the degradation rate but burdens the device mass and cost (Lozinski *et al.* 2019; Plis *et al.* 2021). GEO and MEO satellites are more sensitive to the ESD effects.

In addition, solder joints may be cracked under the highly repeated temperature alternation leading to the circuit off (Navarro *et al.* 2020). In the lower orbit, spacecrafts should also pay attention to the atomic oxygen (AO) effects damaging the solar cell interconnects (Zhu *et al.* 2019). For LEO satellites, although the Earth albedo can increase the solar array output power to make the energy supply more advantageous, the longtime output power of the solar array continues to decrease in the space environments. With the popularly rapid development of the electric propulsion technology, the plume contamination becomes another focus of SEEs (Nuwal *et al.* 2020) because of molecular contaminants darkening the the solar cell glass cover. Molecular contamination effects can be intensified when ultraviolet (UV) effects are enhanced.

**Corresponding Author: Yu Jiang:** State Key Laboratory of Astronautic Dynamics, China Xi'an Satellite Control Center, Xi'an 710043, China; Email: jiangyu_xian_china@163.com
**Qiang Li, Yan Zhang, Yu Gao, Xiaohong Guo, Ruifei Cui, Sichen Wang, Wenming Guo, Tiexin Lv, Lifeng Cai, Lei Zhang, Xiaoying Li, Haichen Lin:** State Key Laboratory of Astronautic Dynamics, China Xi'an Satellite Control Center, Xi'an 710043, China

However, how to deal with the solar cell power loss in space operation is seldom mentioned in the literature. In fact, effectively trying to mitigate the energy shortage impacts in the satellite power systems has always been an effort made by the space operation engineers to extend the payload life on orbit.

It is known that attitude determination and control system (ADCS) can provide navigation assistance to LEO satellites with attitude measurement, determination and control (Soken *et al.* 2020; Fieseler *et al.* 2020; Chujo *et al.* 2020; Wang *et al.* 2021). Navigation assistance can be used to control the attitude for both the satellite and other subsystems, such as payloads, solar arrays, etc (Magner *et al.* 2020; O'Reilly *et al.* 2021; Llaveria *et al.* 2020; Golpashin 2020). In the light of this way, solar panel direction to the Sun can be adjusted by the ADCS to vary the solar cell output power.

In view of the energy budgets, an LEO satellite confronted with the risks of power insufficiency resulted from the solar array output degradation is sampled. An attitude control method is presented to maneuver the yaw angle to effectively improve the solar array supply. The second part of the paper mainly analyzes the telemetry data variations of the currents and the temperatures from the solar array and proposes a yaw control scheme. In the third part, models of the orbit incidence and the panel incidence are built to simulate the improvements of the power supply. The fourth part calculates the yaw angle and angular velocity in the attitude maneuver. The fifth part shows the results in space operation, and the yaw maneuver differences from the simulation calculated to the telemetry observed are discussed. The sixth part is a conclusion.

## 2 Telemetry parameter variations of the solar array

An LEO satellite running on a Sun synchronous orbit (SSO) has an initial orbit height of about 493.1 km, an inclination of about 97.4°, an eccentricity close to 0, and a local time of descending node (LTDN) near 06:00 AM. The LTDN variations of the satellite orbit are shown in Figure 1. The horizontal MJD is a day count starting from January 1, 2000, in Figure 1. It can be seen that the LTDN is varying around 06:00 AM and the satellite orbit is dawn-dusk. The LTDN changes have an annual period with minima in February, July and maxima in May, October, and are related to the secular drifts of the right ascensions of the ascending node and the Sun (Mortazavi 2015).

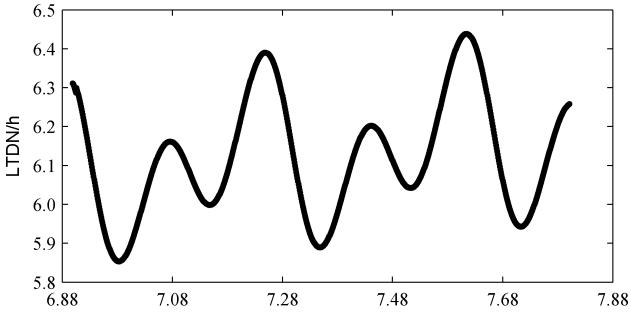


**Figure 1.** LTDN variations

Here, the orbital normal ***OH*** is defined as a unit vector in the celestial sphere, and the ***O*** point is the Earth center. Obviously, when the SSO is a dawn-dusk orbit with the LTDN near 06:00AM, ***OH*** points to the side of the Sun. Furthermore, ***OS*** is also defined as a unit vector from the Earth to the Sun in the celestial sphere, and ***S*** is the solar nadir. The angle between ***OS*** and ***OH*** is defined as the orbit incidence, $\theta$. Figure 2 shows the orbit incidence variations that have a yearly characteristic with a minimum value in February and a maximum value in June. Similarly, the solar cell panel normal ***ON*** is defined as another unit vector in the celestial sphere, and the angle between ***OS*** and ***ON*** is defined as the panel incidence.

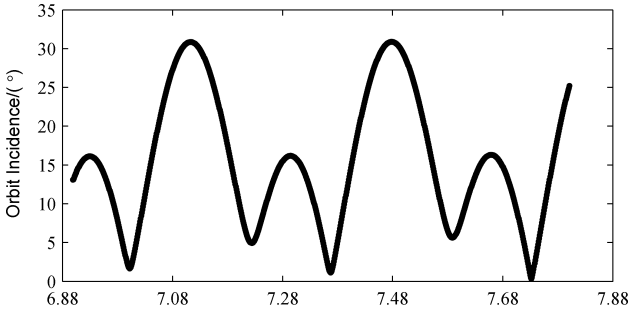


**Figure 2.** Variations of the orbit incidence

Figure 3 plots the satellite orbit on the celestial sphere and the point A is the satellite nadir. It is clear that the solar light is almost perpendicular to the orbital plane to be instrumental in equipping the solar array. When the solar cell panel is parallel to the satellite orbit plane, it can be fixed mounting with no rotating joints and slip rings to enhance the reliability of the spacecraft energy subsystem (Sun *et al.* 2020). In this instance of fixed mounting, while the attitude angles are zeros, ***OH*** and ***ON*** coincide with each other.

However, the SEEs exert continuously strong impacts on the LEO satellite solar array at the risk of losing the power

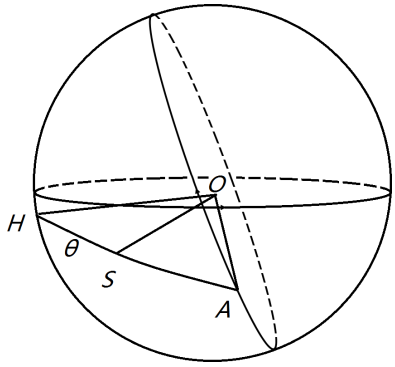


**Figure 3.** Celestial sphere

output. The solar array output currents of the LEO satellite on orbit are illustrated in Figure 4. Here, the telemetry data time is selected near the equinoxes and solstices, and each is sampled on March 22nd, June 22nd, September 22nd and December 22nd. The horizontal axis, Js, is a cumulative second count of one day.

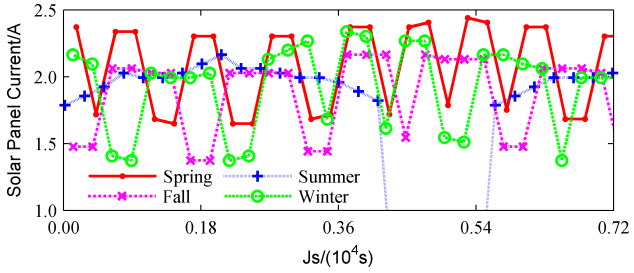


**Figure 4.** Current telemetry values of solar array

As can be seen from Figure 4, the maximum current appears near the vernal equinox, and the current reaches the lowest level in the summer solstice. This is because that near the summer solstice, there are Earth shadows in the satellite orbit and the solar array outputs zeroes in the shadows. In addition, referred to Figure 2, we can see that the orbit incidence in June is at the top level that can give rise to the lowest output.

In the winter solstice, the orbit incidence is obviously smaller than that in the vernal equinox in Figure 2. However, the winter solstice current is smaller and not bigger than the vernal equinox current. This may indicate that the current drop is rapid and and the solar array performance may be significantly affected by the SEEs. Especially during the summer, the orbital sunshine is the worst in the whole year. Due to the Earth shadows, the LEO satellite requires the batteries to supply the power. Therefore, in space operation, we need to focus on the solar energy input changes near the summer solstice, and pay attention to the satellite state of health (SOH).

## 3 Models of the orbit incidence and the panel incidence

According to the solar cell output degradation, the power variation factors are investigated, and the countermeasures in space operation are put forward.

The output power of a monolithic solar cell can be expressed as (Conibeer and Willoughby 2014; Patel 2010):

$$\begin{aligned} P &= FUI \\ U &= U_0[1 + k_U(T - 25)] \\ I &= I_0[1 + k_I(T - 25)]\cos b \end{aligned} \tag{1}$$

where $P$ is the output power, W; $U$ is the working voltage of the cell, V; $U_0$ is the open circuit voltage under the condition of AM0 which means that the solar power is 1353 W m$^{-2}$ at the temperature of 25°C, V; $I$ is the working current, A; $I_0$ is the short-circuit current under the AM0 condition, A; $k_U$ is the thermal coefficient of the voltage, V K$^{-1}$, which is generally negative. $k_I$ is the thermal coefficient of the current, A K$^{-1}$, usually positive. $T$ is the working temperature, K; $b$ is the panel incidence and $F$ is a power factor. In general, $k_U$ and $k_I$ are negative and positive, respectively.

The power factor is mainly affected by the following items: Sun-Earth distance, Earth albedo, occlusion shadow, light source, space environment, etc. Among these factors, the variation of the Sun-Earth distance is relatively regular, and the solar power density is the highest while the distance is the shortest at the perihelia. For an LEO satellite, the influences of the Earth albedo are relatively clear, especially when the satellite runs over in the polar regions. Occlusion shadow is generally considered in the satellite design before launched and is cautioned in the attitude maneuvers on orbit. In the visible wave band, the solar power is stable, and the fluctuation is always neglected. However, the space environmental factor is relatively complex with cumulative and transient radiation effects and unexpected events, especially the extreme space weather events.

The panel incidence, $b$, plays a vital role in varying the solar cell power. When $b$ is 0, the output is the top. When $b$ equals 90°, the output is 0. Therefore, we present an orbital proposal to adjust the panel incidence by controlling the yaw angle. The panel incidence model is shown in Figure 5.

In Figure 5, based on the satellite orbit plane, a reference coordinate frame $\boldsymbol{OX_rY_rZ_r}$ is established. Here, $\boldsymbol{OZ_r}$ is $\boldsymbol{OH}$ that is the orbital normal in Figure 3, $\boldsymbol{OX_r}$ is $\boldsymbol{OA}$ on the

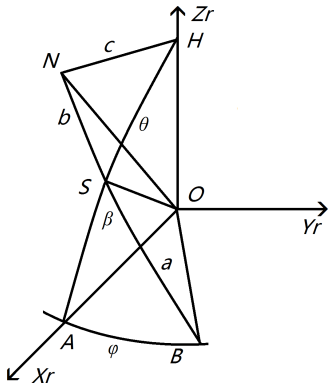


**Figure 5.** Model of the panel incidence

plane consisting of ***OS*** and ***OH***, and ***OY***$_r$ given by the right hand rule is ***OZ***$_r$ × ***OX***$_r$.

Assuming that the satellite moves from the initial position ***A*** to the point ***B***, the angle between ***OA*** and ***OB*** is defined as the orbital phase, $\varphi$. When the satellite arrives at the point ***B***, ***OB*** is the yaw axis. Rotating ***OB*** makes ***ON*** that is the panel normal, ***OS*** and ***OB*** on the same plane with a yaw angle, $c$. The angle $a$ is between ***OS*** and ***OB***. The angle $b$ is the panel incidence between ***OS*** and ***ON***, $\theta$ is the orbit incidence, and $\beta$ is the angle between the plane ***ONSB*** and the plane ***OHSA***.

It can be seen that ∠***BAS*** and ∠***HNS*** are equal to 90°. For ***BAS*** and ***HNS*** are right spherical triangles, equations can be expressed as followed:

$$\sin a = \frac{\sin\varphi}{\sin\beta} \tag{2}$$

$$\cos a = \cos\varphi \sin\theta \tag{3}$$

$$\sin\theta = \frac{\sin c}{\sin\beta} \tag{4}$$

$$\cos\theta = \cos b \cos c \tag{5}$$

According to Eq. (5), the panel incidence, $b$, can be described as:

$$\cos b = \frac{\cos\theta}{\cos c} \tag{6}$$

Considering that cos $c$ is less than 1, we can see that $b$ is lower than $\theta$ and, the panel incidence is smaller than the orbit incidence to increase the solar energy input.

From Eq. (2) to Eq. (5), $b$ and $c$ can be written as:

$$\cos b = \sqrt{1 - \cos^2\varphi\sin^2\theta} \tag{7}$$

$$\sin c = \frac{\sin\varphi\sin\theta}{\sqrt{1 - \cos^2\varphi\sin^2\theta}} \tag{8}$$

Figure 2 draws the orbit incidence variations. Here, with consideration of secular orbit drifts, the varying panel

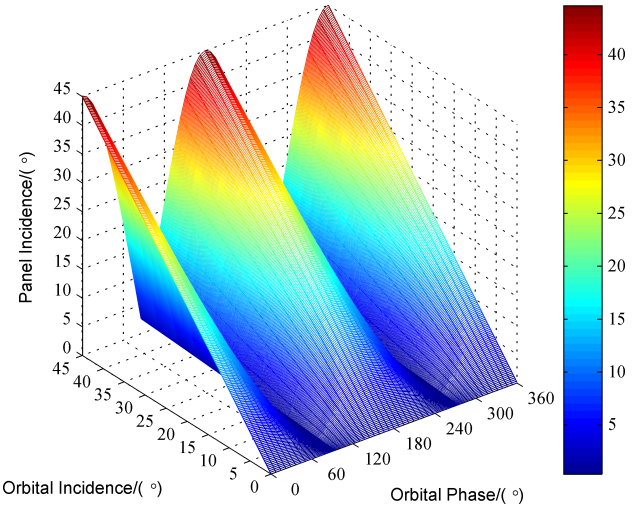


**Figure 6.** Simulations of the panel incidence

incidence simulation is mapped in Figure 6 and the orbital angle is the orbital phase, $\varphi$, from Figure 5.

The results in Figure 6 show that after the yaw control, the panel incidence is lower than the orbit incidence to improve the the solar input while the satellite is running on orbit.

Here, we give a definition as:

$$\eta = \frac{1}{2\pi}\int_0^{2\pi}\frac{\sqrt{1 - \cos^2\varphi\sin^2\theta}}{\cos\theta}d\varphi = \frac{2}{\pi}\int_0^{\pi/2}\frac{\sqrt{1 - \cos^2\varphi\sin^2\theta}}{\cos\theta}d\varphi \tag{9}$$

In Eq. (9), $\eta$ is an averaged ratio of cos $b$ and cos $\theta$ from Eqs of (7) and (8) with an orbital period integral. Deriving $\eta$ with respect to $\theta$ is:

$$\frac{d\eta}{d\theta} = \frac{2}{\pi}\int_0^{\pi/2}\frac{\sin^2\varphi\sin\theta}{\cos^2\theta\sqrt{1 - \cos^2\varphi\sin^2\theta}}d\varphi \tag{10}$$

Eq. (10) shows that the derivative, d$\eta$/d$\theta$, is positive because of $0 < \theta < 90°$, and indicates that $\eta$ is an increasing function of $\theta$. The numerical integration results of Eq. (9) are shown in Figure 7.

From Figure 7, we can see that when the orbit incidence, $\theta$, is varying from 30° to 35°, the ratio $\eta$ is increasing from 1.08 to 1.11. This indicates that as the orbit incidence increment is more, the yaw maneuver to improve the panel incidence will be more efficient.

In Eq. (8), the angle $c$ is the yaw angle $\psi$:

$$\psi = c \tag{11}$$

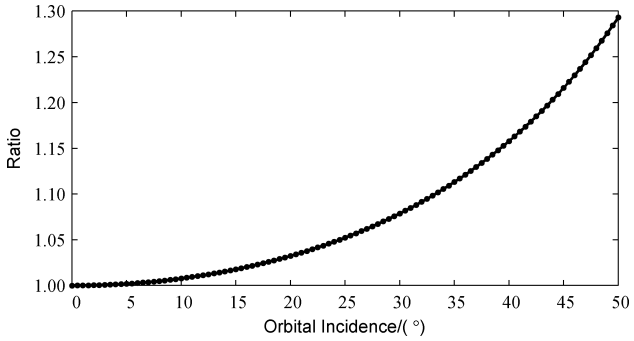


**Figure 7.** Ratio simulations of the orbit incidence

It is assumed that the time when the satellite is at point $A$ is $t_0$ equaling 0, and the orbital angular velocity of the satellites is $\omega_o$. When the satellite arrives at point $B$ at the time $t$, the orbital phase $\varphi$ is:

$$\varphi = \omega_o t \tag{12}$$

From Eqs. (8), (11) and (12), the yaw rate $\omega_z$ can be presented as:

$$\omega_z = \frac{d\psi}{dt} = \frac{\omega_o}{2} \frac{\cos \omega_o t \sin 2\theta}{1 - \cos^2 \omega_o t \sin^2 \theta} \tag{13}$$

Similarly, when the orbit incidence is varying from 0° to 35°, with the orbital height of 491.3 km and the eccentricity approximately equaling to zero, the simulation results of the yaw angle and the yaw angular velocity are shown in Figure 8 and Figure 9.

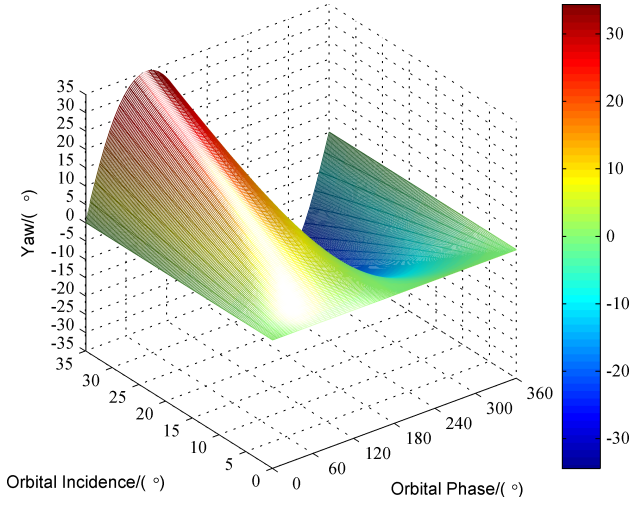


**Figure 8.** Simulations of the yaw angle

As shown in Figures 8 and 9, the yaw angle and angular velocity in amplitude will increase with the rise of the orbit incidence. For example, in the summer solstice, the yaw

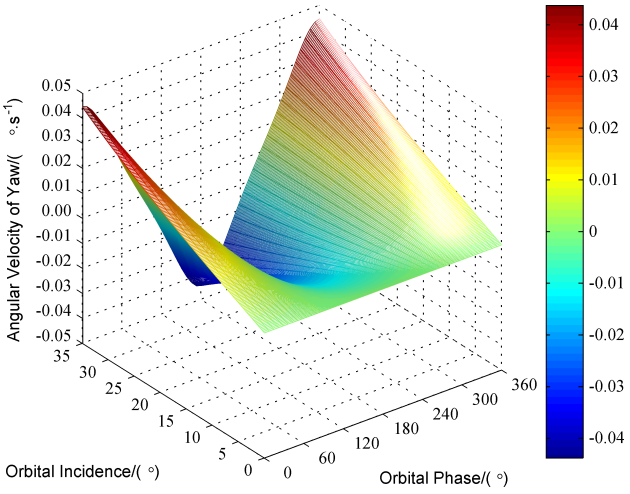


**Figure 9.** Simulations of yaw angular velocity

angle amplitude reaches the extrema at $\varphi = \pm 90°$:

$$\begin{aligned} \psi_{\max} &= \theta, \quad (\varphi = 90°); \\ \psi_{\min} &= -\theta, \quad (\varphi = -90°) \end{aligned} \tag{14}$$

At the same time, the yaw rate amplitude comes to the extrema at $\varphi = 0$ and 180°, respectively:

$$\begin{aligned} \omega_{z\max} &= \omega_o \tan\theta, \quad (\varphi = 0); \\ \omega_{z\min} &= -\omega_o \tan\theta, \quad (\varphi = 180°) \end{aligned} \tag{15}$$

In Figure 9, when $\theta$ is 35°, the maximum and minimum values of yaw angular velocity are 0.0445° $s^{-1}$ and −0.0445° $s^{-1}$, respectively.

From the simulation results, we can see that the yaw control is effective to enhance the solar cell output. light angle of windsurfing can be improved under yaw control and can be applied to attitude control. Next, the attitude control simulation is investigated with the orbital elements to simulate the yaw maneuver.

# 4 Simulations of the yaw maneuver

Before calculating the yaw angle and angular velocity of attitude control, it is necessary to define the coordinate systems first. Here, J2000.0 inertial coordinate system, orbital coordinate system and body coordinate system are mainly considered:

In the J2000.0 inertial coordinate system $\boldsymbol{OX_IY_IZ_I}$, the origin $O$ is the Earth center, $\boldsymbol{OX}_I$ is pointing to the vernal equinox, $\boldsymbol{OZ}_I$ is the equator normal, $\boldsymbol{OY}_I$ is determined by the right hand rule.

In the orbital coordinate system $\boldsymbol{OX_oY_oZ_o}$, $O$ is the satellite centroid, $\boldsymbol{OZ}_o$ points to the Earth center, $\boldsymbol{OY}_o$ is the

opposite direction of the orbital normal, $\boldsymbol{OX}_o$ is determined by the right hand rule.

The body coordinate system is $\boldsymbol{OX}_b\boldsymbol{Y}_b\boldsymbol{Z}_b$, when the three axis attitude angles are 0, $\boldsymbol{OX}_b\boldsymbol{Y}_b\boldsymbol{Z}_b$ and $\boldsymbol{OX}_o\boldsymbol{Y}_o\boldsymbol{Z}_o$ coincide.

Assuming that the solar right ascension and the solar declination are $\alpha_s$ and $\delta_s$ in J2000.0 coordinate system, respectively, the Earth-Sun vector $\boldsymbol{OS}_0$ can be formulated as:

$$\boldsymbol{OS}_0 = \begin{pmatrix} \cos\alpha_s\cos\delta_s & \sin\alpha_s\cos\delta_s & \sin\delta_s \end{pmatrix}^T \tag{16}$$

In the orbital elements of the J2000.0, the right ascension of descending node is $\Omega$, the inclination is $i$, the perigee angle is $\omega$, and the true anomaly is $f$. The vector $\boldsymbol{OS}_0$ can be transformed from the J2000.0 coordinate system to the orbit coordinate system.

First, by rotating $\Omega$ around $\boldsymbol{OZ}_I$, the rotation matrix $\boldsymbol{R}_z(\Omega)$ is:

$$R_z(\Omega) = \begin{pmatrix} \cos\Omega & \sin\Omega & 0 \\ -\sin\Omega & \cos\Omega & 0 \\ 0 & 0 & 1 \end{pmatrix} \tag{17}$$

Secondly, rotating $i$ around the $\boldsymbol{X}$ axis presents the rotation matrix $\boldsymbol{R}_x(i)$:

$$R_x(i) = \begin{pmatrix} 1 & 0 & 0 \\ 0 & \cos i & \sin i \\ 0 & -\sin i & \cos i \end{pmatrix} \tag{18}$$

Thirdly, rotation of $\omega + f$ around the $\boldsymbol{Z}$ axis gives the rotation matrix $\boldsymbol{R}_z(\omega + f)$:

$$R_z(\omega+f) = \begin{pmatrix} \cos(\omega+f) & \sin(\omega+f) & 0 \\ -\sin(\omega+f) & \cos(\omega+f) & 0 \\ 0 & 0 & 1 \end{pmatrix} \tag{19}$$

Then, rotating $-90^\circ$ around the Y axis makes the rotation matrix $\boldsymbol{R}_y(-90^\circ)$:

$$R_y(-90^\circ) = \begin{pmatrix} 0 & 0 & 1 \\ 0 & 1 & 0 \\ -1 & 0 & 0 \end{pmatrix} \tag{20}$$

Finally, by rotating $90^\circ$ around the Z axis, the rotation matrix $\boldsymbol{R}_z(90^\circ)$ is:

$$R_z(90^\circ) = \begin{pmatrix} 0 & 1 & 0 \\ -1 & 0 & 0 \\ 0 & 0 & 1 \end{pmatrix} \tag{21}$$

The new vector $\boldsymbol{OS}$ can be expressed as:

$$OS = \begin{pmatrix} x_s & y_s & z_s \end{pmatrix}^T \tag{22}$$

According to Eqs. (17-22), we can write $\boldsymbol{OS}$ as:

$$OS = R_z(90^\circ)R_y(-90^\circ)R_z(\omega+f)R_x(i)R_z(\Omega)OS_0 \tag{23}$$

Eq. (23) can be expanded as:

$$\begin{aligned} x_s = &-\cos\alpha_s\cos\delta_s\left(\sin(\omega+f)\cos\Omega\right. \\ &\left.+\cos(\omega+f)\cos i\sin\Omega\right) \\ &-\sin\alpha_s\cos\delta_s\left(\sin(\omega+f)\sin\Omega-\cos(\omega+f)\cos i\cos\Omega\right) \\ &+\sin\delta_s\cos(\omega+f)\sin i \end{aligned} \tag{24}$$

$$\begin{aligned} y_s = &-\cos\alpha_s\cos\delta_s\sin i\sin\Omega \\ &+\sin\alpha_s\cos\delta_s\sin i\cos\Omega-\sin\delta_s\cos i \end{aligned} \tag{25}$$

$$\begin{aligned} z_s = &-\cos\alpha_s\cos\delta_s\left(\cos(\omega+f)\cos\Omega\right. \\ &\left.-\sin(\omega+f)\cos i\sin\Omega\right) \\ &-\sin\alpha_s\cos\delta_s\left(\cos(\omega+f)\sin\Omega+\sin(\omega+f)\cos i\cos\Omega\right) \\ &-\sin\delta_s\sin(\omega+f)\sin i \end{aligned} \tag{26}$$

Figure 10 shows the Earth-Sun vector $\boldsymbol{OS}$ in the orbital coordinate system. After rotating $\psi$ around the $\boldsymbol{OZ}_o$, $\boldsymbol{OS}$, $\boldsymbol{OZ}_o$, and the panel normal $\boldsymbol{ON}$, are on the same plane. When the attitude angles are zeroes before the rotation, $\psi$ is the yaw that can be achieved by rotating around the $\boldsymbol{OZ}_b$ axis.

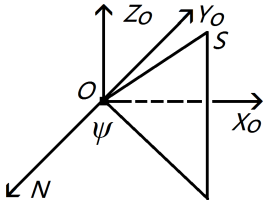


**Figure 10.** Geometric model on orbit coordinate system

From Figure 10, The yaw, $\psi$, can be calculated as:

$$\psi = -\text{atan}\frac{x_s}{y_s} \tag{27}$$

Figures 11 and 12 illustrate the yaw angle and the yaw angular velocity which are calculated with the orbital elements near the equinoxes and the solstices in 2020.

It can be seen that the yaw angle and angular velocity amplitudes are the highest near the summer solstice. The yaw angular velocities of Figure 11 and Figure 8, and the yaw angular velocities of Figure 12 and Figure 9 are basically the same in the numerical intervals to indicate that the models and the simulations are agreeable.

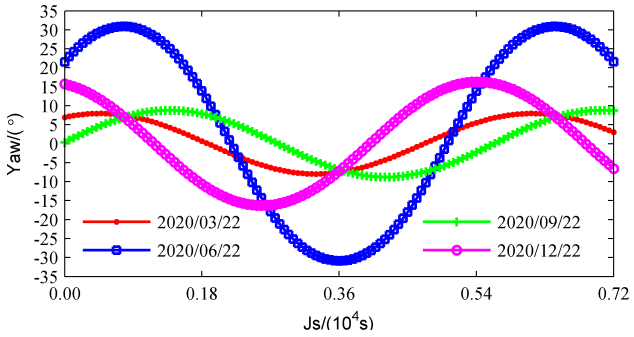


**Figure 11.** Simulations of the yaw angle with orbital elements

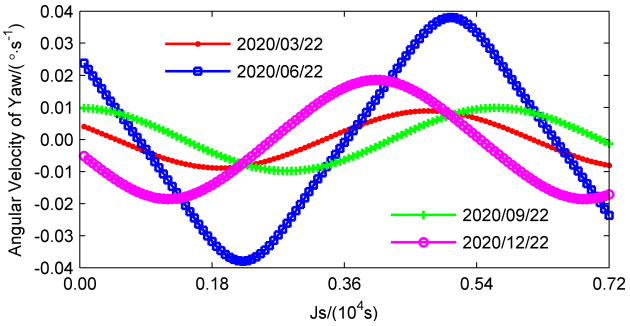


**Figure 12.** Simulations of the yaw angular velocity with orbital elements

## 5 Results and discussions

In space operation, a yaw maneuver implementation is used to heighten the electric power supply (EPS) output to meet the solar cell degradation due to the SEEs. By controlling the yaw attitude, vectors ***ON*** that are the solar panel normal, $\boldsymbol{OZ}_b$ that belongs to the body coordinate system, and ***OS*** pointing to the Sun from the Earth are on the same plane in the celestial sphere.

Control results of the yaw maneuver from the first day are shown in Figure 13 and 14 with the yaw angle and the yaw angular velocity. The observed are the telemetry data in the downlink from the satellite ADCS, the calculated are the simulation data using the orbital elements. In the calculated data, the yaw angular velocity is a numerical differentiation from the yaw angle. As can be seen, the theoretical calculations are indeed in good agreement with the telemetry observations to indicate the modelling and the simulating are correct and the ADCS works well.

Figures 15 and 16 illustrate the results of the solar panel temperature and current before and after the yaw control.

As shown in Figure 15, the thermal fluctuation range after the control is obviously smaller and the amplitude is reduced from 83.7°C to 61°C. According to Eq. (1), we can see that the decrease of the temperature range is helpful

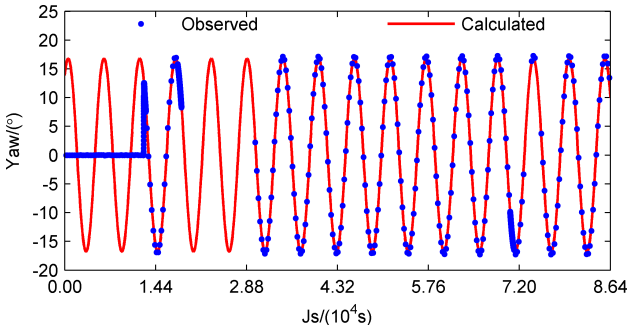


**Figure 13.** Observed and calculated results of the yaw angle

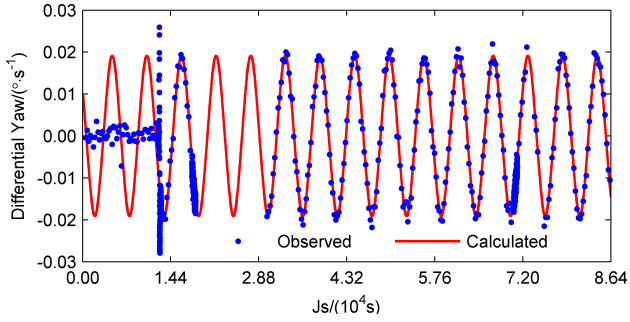


**Figure 14.** Observed and calculated results of the yaw angular velocity

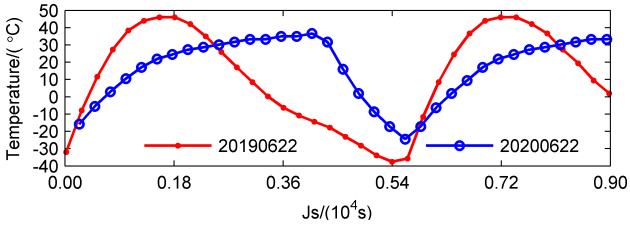


**Figure 15.** Temperature variations of the solar array

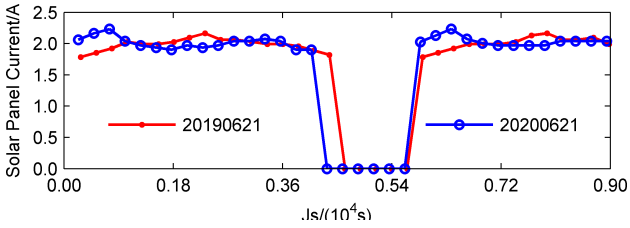


**Figure 16.** Current variations of the solar array

to improve the power output stability. At the same time, the thermal peaks become lower, and the thermal valleys are higher. The temperature difference in an orbital period drops to mitigate the thermal stress impacts on the solar cells in the space irradiation environments to improve the device reliability.

As can be seen from Figure 16, the maximum and minimum values of the solar cell current in the sunshine area

are 2.16A and 1.79A before the yaw maneuver, and the average value is about 2.00A. After the space operation, the maximum, minimum and averaged values are 2.23A, 1.90A and 2.03A.

The average values are compared here to evaluate the yaw mode effects. In fact, the mean current of 2.03A is the result after the maneuver. If there is no attitude control, the mean value should be even smaller. Referring to the data in Figure 7, the ratio parameter, $\eta$, is 1.079 in Figure 16 in the yaw mode. It can be calculated that the mean current in sunshine area without the attitude maneuver should be 1.88A. This proves that after one year time, the output current from the solar panel rapidly falls from 2.00A to 1.88A with a decrease of 0.12A, and the annual degradation is about 5.9%.

Eq. (1) shows that the solar cell current is determined by several factors containing the panel incidence. Here, the yaw control is employed to reduce the the panel incidence to increase the solar array power. At the same time, solar activities cannot change the direction from the Sun to the Earth and the attitude maneuver is valid all the year.

Xu (2001) detailed an attitude control case about FY-1B satellite which had exhausted the fuel and was rescued by employing the geomagnetic field and the gravity field. Peng *et al.* (2008) reported a posture anomaly handling process that an LEO satellite which had one tank of fuel emptied and the other frozen was damped by the geomagnetic field to recover. Other examples described by Desouky and Abdelkhalik (2020); Huang *et al.* (2018); Cubas and De Ruiter (2020) also show the attitude handling from different satellites mainly using the magnetic damping for detumbling.

Therefore, the ADCS plays an extremely important role in the spacecraft management and maintenance. In space operation, it is necessary to excavate the ADCS performance to play its maximum role to provide assistance for satellite operation or life extension. Bitetti *et al.* (2018) believed that the satellite life extension is an optimized output result that comprehensively considers fuel, energy, thermal control, and space environment constraints. Iovine (2018) and Chambliss (2018), respectively, summarized the on-orbit maintenance work of the International Space Station (ISS), and they pointed out that good thermal management and control play a vital role in reliability and life extension; Zhang (2020) thought that the refinement of space manipulation helps to improve the management level of overdue spacecraft. In this paper example, in view of the influence of the SEEs on the solar cell array power degradation, the ADCS is used to implement the yaw maneuver, so that the the solar cell output current is increased, and the thermal stress is reduced, and the impacts of the SEEs are effectively mitigated.

In addition, radiation hardening by design (RHBD) for the SEEs is another key attention. Nowadays, in the near-Earth space, the spacecraft number is rapidly increasing in quantities (Kopacz *et al.* 2020; Anderson *et al.* 2020) and the space applications of commercial off-the-shelf (COTS) devices have become increasingly widespread (You *et al.* 2019; Bai 2019). However, Zhang *et al.* (2019) and Gohardani (2018) emphasized that the radiation protection is critical and must be seriously taken into account to meet the space application requirements because that the COTS ICs are often vulnerable to the SEEs. In the following work, it is necessary to pay more attention to the space environment impacts on other devices or subsystems for telemetry diagnosis, state of health (SOH) management and orbital maintenance.

# 6 Conclusions

In this study, with respect to the solar cell power degradation due to the SEEs, a yaw control method is implemented on orbit to effectively improve the panel incidence to increase the solar cell output current. In the summer solstice, when the orbit incidence is 30°, the yaw maneuver can give a ratio rise of about 8% in the current. While the orbit incidence is 35°, the current increasing ratio will reach more than 10%.

The yaw control can be conveniently used to harvest more solar power to meet the energy requirements for other satellites running in the near-Earth space.

In the future, if the solar array performance continues to deteriorate, it is also possible to add a roll maneuver based on the yaw control, which is expected to further improve the solar cell output.

**Acknowledgment:** This project is funded by National Natural Science Foundation of China (No. 11772356).

**Author contributions:** All authors have accepted responsibility for the entire content of this manuscript and approved its submission.

**Conflict of interest:** The authors state no conflict of interest.

## References


Anderson MA, Duron CM, Farmer TA, Hitt MA, Klinner MG, Lanz GE, et al. Army decade in space. 34th Annual AIAA/USU Conference on Small Satellites. 2020.

Bai ZG. 2019. Development achievements and prospects of China modern small satellite. Hangtianqi Gongcheng. 28(2):1–8.

Bitetti L, Ratti BB, Destefanis R, Sanchez AH. Reliability model supporting satellite life extension and disposal operations initiation. 2018 SpaceOps Conference. 2018 May 28- June 1; Marseille, France. AIAA; 2018.

Chambliss J. The ISS TCS system manager experience. 48th International Conference on Environmental Systems. 2018 July 8-12; Albuquerque, USA. 2018.

Chujo T, Watanabe M, Mori O. 2020. Mechanism-free control method of solar/thermal radiation pressure for application to attitude control. Astrodynamics. 4(3):205–222.

Conibeer GJ, Willoughby A. 2014. Solar cell materials: developing technologies. John Wiley & Sons Ltd.

Cubas J, De Ruiter A.2020. Magnetic control without attitude determination for spinning spacecraft. Acta Astronaut. 169(1):108–123.

Desouky MAA, Abdelkhalik O. 2020. Time-optimal magnetic attitude detumbling. J Spacecr Rockets. 57(3):549–564.

Engelhart DP, Plis EA, Ferguson DC, Artyushkova K, Wellems D, Cooper R, Hoffmann R. 2019. XPS investigation of the source of GPS arc contamination. IEEE Trans Plasma Sci. 47(8):3848–3851.

Espinet-Gonzalez P, Barrigon E, Yang C, Otnes G, Vescovi G, Mann C, et al. 2020. Nanowire solar cells: a new radiation hard PV technology for space applications. IEEE Int J Photovolt. 10(2):502–507.

Ferguson DC, Plis EA, Hoffmann RC, Engelhart DP. A proven method to prevent solar array arcing in GEO-bulk-conductive coverglasses. AIAA Scitech 2020 Forum. 2020 Jan 6-10; Orlando, USA. AIAA; 2020.

Ferguson DC, Perillat P, Plis EA, Vayner B. 2020. Statistical properties of arcing on GPS pseudo random noise 28. J Spacecr Rockets. 57(3):405–412.

Ferguson DC, White S, Rast R, Holeman E. 2019. The case for global positioning system arcing and high satellite arc rates. IEEE Trans Plasma Sci. 47(8):3834–3841.

Fieseler PD, Taylor J, Klemm RW. 2020. Dawn spacecraft performance: resource utilization and environmental effects during an 11-year mission. J Spacecr Rockets. 57(1):147–159.

Gohardani AS. Small satellites: observations and considerations. 2018 AIAA Aerospace Sciences Meeting. 2018 Jan 8-12; Kissimme, Florida. 2018.

Golpashin AE, Yeong HC, Ho K, Sri N. 2020. Spacecraft attitude control: a consideration of thrust uncertainty. J Guid Control Dyn. 43(12):2349–2365.

Gueymard CA. 2018. A reevaluation of the solar constant based on a 42-year total solar irradiance time series and a reconciliation of spaceborne observations. Sol Energy. 168:2–9.

Hands ADP, Ryden KA, Meredith NP, Glauert SA, Horne RB. 2018. Radiation effects on satellites during extreme space weather events. Space Weather. 16(8):1216–1226.

Huang MX, Hong MY, Juang JC. Analysis of tumbling motions by combining telemetry data and radio signal. 32nd Annual AIAA/USU Conference on Small Satellites. AIAA; 2018.

Iovine JV. International space station passive thermal control system top ten lessons-learned. 48th International Conference on Environmental Systems. 2018 July 8-12; Albuquerque, USA. 2018.

Kerr E, MacDonald M. 2021. Limits of drag augmentation at spacecraft end-of-mission and a mitigation strategy. Astrodynamics. 5(2):109–120.

Keys C, Watkins B, Coughlin C, Hoang B, Beyene S. MAXAR EOR radiation to power predictions. AIAA Scitech 2020 Forum AIAA. 2020 Jan 6-10; Orlando, USA. AIAA; 2020.

Kopacz J, Herschitz R, Roney J. 2020. Small satellites an overview and assessment. Acta Astronaut. 170(1):93–105.

Llaveria D, Camps A, Park H. 2020. Correcting the ADCS jitter induced blurring in small satellite imagery. IEEE Journal on Miniaturization for Air and Space Systems. 1(2):130–137.

Lozinski AR, Horne RB, Glauert SA, Zanna GD, Evans HDR. 2019. Solar cell degradation due to proton belt enhancements during electric orbit raising to GEO. Space Weather. 17(7):1059–1072.

Lu YF, Shao Q, Yue HH, Yang F. 2019. A review of the space environment effects on spacecraft in different orbits. IEEE Access. 7:93473–93488.

Magner R, Roth N, Cotten B, Zee RE. Guidance, navigation, and control for agile small spacecraft with articulating solar arrays. 34th Annual AIAA/USU Conference on Small Satellites. 2020; Logan, USA.

Maurer RH, Goldsten JO, Peplowski PN, Holmes-Siedle AG, Butler MH, Herrmann CC, et al. 2018. Five - year results from the engineering radiation monitor and solar cell monitor on the Van Allen probes mission. Space Weather. 16(10):1561–1569.

Mortazavi SH. Orbit selection trade-offs for LEO observation microsatellites. AIAA Space 2015 Conference and Exposition. 2015 Aug 31-2 Sep; Pasadena, USA. AIAA; 2015-4501:1-16.

Navarro M, Gussy J, Pack D, Rowen D, Salvaggio D. Building satellites in 18 months: lessons learned from the rogue alpha/beta CubeSats. 34th Annual AIAA/USU Conference on Small Satellites.2020; Logan, USA.

Nuwal N, Jambunathan R, Levin DA. 2020. Kinetic modeling of spacecraft surfaces in a plume backflow region. IEEE Trans Plasma Sci. 48(12):4305–4325.

O'Reilly D, Herdrich G, Kavanagh DF. 2021. Electric propulsion methods for small satellites: a review. Aerospace (Basel). 8(1):22.

Patel MR. (Han B. Translated). 2010. Spacecraft power systems. China Astronautics Press.

Peng RJ, Ma XY, Zheng KY, Wang WY. 2008. On-orbit fault repair and recovery of a low orbit satellite. Hangtianqi Gongcheng. 17(1):24–29.

Plis EA, Engelhart DP, Murray VJ, Sokolovskiy AN, Hoffmann RC. 2021.Effect of simulated GEO environment on the properties of solar panel coverglasses. IEEE Trans Plasma Sci. 49(5):1679–1685.

Soken HE, Sakai S-I, Asamura K, Nakamura Y, Shinohara I. 2020. Filtering-based three-axis attitude determination package for spinning spacecraft: preliminary results with arase. Aerospace (Basel). 7(7):97.

Sun YH, Yu JB, Liu XJ, Sun XW, Wang YS. 2020. Reliability evaluation of wear failure simulation of conductive slip ring under small sample. J Astronaut. 41(5):624-632.

Toyoda K, Kose S, Sasaki T, Cho M. Difference in threshold voltage of arc inception between electron beam and ultraviolet environment. AIAA Scitech 2020 Forum. 2020 Jan 6-10; Orlando, USA. AIAA; 2020.

Wang LY, Guo YN, Ma GF, Liu WL. 2021. Review on input saturation in the spacecraft attitude control. Journal of Astronautics. 42(1):11–21.

Xapsos M. 2019. A brief history of space climatology: from the big bang to the present. IEEE Trans Nucl Sci. 66(1):17–37.

Xu FX. 2001. Technique of successful rescue of FY-1B meteorological satellite by using the geomagnetic field and the gravitational field. J Astronaut. 22(2):1-11.

You Z, Shi S, Zhao KC, Xing F, Zhang GF, Zhou B, et al. 2019. Key technologies for research & development of nanosatellite. Hangtianqi Gongcheng. 28(1):1–9.

Zhang ZG. 2020. Refined practice of in-orbit management for overdue spacecraft. Hangtianqi Gongcheng. 29(2):109–114.

Zhang HW, Li PW, Sun Y. 2019. Investigation on radiation hardness assurance for components' performance in commercial aviation space. Hangtianqi Gongcheng. 28(6):81–86.

Zhu LY, Qiao M, Zeng Y, Zhang XF, Liu ZG, Zhang WJ. 2019. Atomic oxygen effect analysis and experimental study of LEO satellite solar cell circuit. Hangtianqi Gongcheng. 28(1):137–142.